Impact of long-range disorder on the two-dimensional electron gas formation at a $LaAlO_3/SrTiO_3$ interface

I. V. Maznichenko,[1,*] S. Ostanin,[1] V. K. Dugaev,[2] I. Mertig,[1,3] and A. Ernst[3,4,5]

[1]*Institut für Physik, Martin-Luther-Universität Halle-Wittenberg, D-06099 Halle, Germany*

[2]*Department of Physics and Medical Engineering, Rzeszów University of Technology, al. Powstańców Warszawy 6, PL-35-959 Rzeszów, Poland*

[3]*Max-Planck-Institut für Mikrostrukturphysik, Weinberg 2, D-06120 Halle, Germany*

[4]*Institute for Theoretical Physics, Johannes Kepler University, Altenberger Straße 69, A-4040 Linz, Austria*

[5]*Donostia International Physics Center (DIPC), E-20018 San Sebastián/Donostia, Basque Country, Spain*

(Received 24 August 2017; revised manuscript received 23 December 2017; published 18 July 2018)

A two-dimensional electron gas (2DEG) can be formed at an interface between two insulators such as $LaAlO_3$ and $SrTiO_3$ without any additional doping. Nevertheless, structural imperfections or defects at the interface, which may arise during the growth process or be of another origin, can definitely affect 2DEG properties either increasing or reducing the 2DEG density. In this work, we study 2DEG formation at both perfect and imperfect interfaces of $LaAlO_3/SrTiO_3$ heterostructures in the framework of the density functional theory. Using a first-principles Green function method within a coherent potential approximation, we investigate consistently the development of the 2DEG density starting from a defectless interface and introducing sequentially various kinds of long-range disorder such as cation intermixing and oxygen vacancies. Finally, we evaluate the 2DEG carrier density from the Fermi surface cross sections and effective masses of the carriers, which may be directly related to the multiple transport phenomena in the system.

DOI: 10.1103/PhysRevMaterials.2.074003

I. INTRODUCTION

Interfaces between robustly insulating perovskites can reveal unexpected metallization [1–3], such as a two-dimensional electron gas (2DEG), observed at $LaAlO_3/SrTiO_3$ (LAO/STO) and discussed mostly in the context of its LaO/TiO_2-terminated (001) interface [4–7]. The nature of this 2DEG is not completely understood so far. In the literature, there are several scenarios, which include (i) the oxygen vacancy-induced mechanism [8], (ii) the La/Sr interfacial mixing [9], and also (iii) the defectless electronic reconstruction, which forms the Ti mixed valence states at the LaO/TiO_2 termination [10]. In view of the most recent experimental findings [11], the focus of discussions around the 2DEG phenomenon at LAO/STO shifts gradually to the intrinsic properties of the TiO_2-terminated interface.

There are a family of composite perovskites for which the LaO/TiO_2 termination is formed unavoidably. In particular, 2DEG appears between STO (001) and $LaFeO_3$ (LFO) [12]. Li *et al.* [13] have reported recently that the crystalline and partially amorphous ABO_3/STO (A = La, Pr, Nd and B = Al, Ga) interfaces become conducting for ABO_3 thicker than four unit cells (u.c.). One of the possible explanations for the critical thickness is significant reconstruction of the crystalline structure at the interface [14]. Density functional theory (DFT) calculations showed that the strong lattice polarization could compensate the dipolar electric field in LAO overlayers and could sustain the insulating behavior up to 5 u.c. LAO. This atomic reconstruction can be prevented by an additional $SrTiO_3$ capping layer at the $LaAlO_3$ surface [15]. It was also proposed to explain this effect by large hopping between cations, which causes the formation of a bound electron state at the interface [16–18]. In the same time, the 2DEG formation can be substantially affected by cation intermixing at the interface and the impact of this effect can strongly depend on the ABO_3 film thickness [12,19–22]. Thus, high crystallinity of the interface is crucial for the defectless mechanism of 2DEG. After oxygen annealing (when the O redox mechanism is removed) the interfaces prepared at 500 °C and below become insulating while samples prepared at 515 °C and above are conducting [13]. Regarding the underlying 2DEG mechanisms, their interplay and critical thickness $\geqslant$4 u.c., needed for 2DEG, the systematic and accurate *ab initio* calculations are required.

One of the explanations of 2DEG, formed at the perfect and stepless (001) interface of LAO/STO, invokes the arguments related to the so-called polar discontinuity [23–26]. Since a LAO (001) heterostructure represents alternately charged planes $[LaO]^+$ and $[AlO_2]^-$, each interfacial La transfers a half of electron into the neighboring and formally neutral TiO_2 layer of an STO substrate. Therefore, the oxidation state of interfacial Ti decreases. The evidence of built-in potential across polar $LaAlO_3$ grown on $SrTiO_3$ substrate has been presented by tunneling measurements between the electron gas and metallic electrodes on $LaAlO_3$ [27]. It shows the presence of an induced dipole moment across the heterostructure. X-ray diffraction technique allows to investigate the atomic structure of different types of interfaces between $LaAlO_3$ and $SrTiO_3$ [28]. These results demonstrated the existence of a polarized region in n-type interface. A direct comparison between

*igor.maznichenko@physik.uni-halle.de

experimental data and *ab initio* calculations for the electrostrictive effect in the polar $LaAlO_3$ grown on $SrTiO_3$ substrates shows a complete screening of the dipole field for film thickness between 6 and 20 unit cells [29]. Direct observation of the electronic structures across oxide interface has been done by using scanning tunneling microscopy and spectroscopy, that confirmed the electronic reconstructions and a built-in electric field in the polar $LaAlO_3$ layer [30]. This scenario of the 2DEG formation for the $Ti^{3.5+}$ valence state and the corresponding *d*-orbital reconstruction was modeled from first principles [8]. It seems that the presence of interfacial La^{3+} and electronically flexible Ti cations is necessary and sufficient to develop the 2DEG effect at a perfect LAO/STO (001) interface. However, all epitaxially grown oxide heterostructures contain intrinsic imperfections such as the oxygen vacancies and substitutional intermixing of cations across the interface [19,20]. Each type of these interfacial defects can induce additional charged carriers, namely, electrons in the case of oxygen vacancies and holes in the case of the Sr substitutes. In addition, the cation intermixing can eliminate the dipolar electric field across the interface and therewith strongly impact the 2DEG formation. In the same time, the presence of defects can lead to an opposite effect, namely, some electrons may become localized and may not participate in the conduction [31]. Also, oxygen vacancies can be responsible or partially responsible for the 2DEG formation. Resonant soft-x-ray measurements performed to investigate electronic structures of $LaAlO_3/SrTiO_3$ superlattices support the oxygen vacancy model [32]. Appearance of magnetism at the $LaAlO_3/SrTiO_3$ interface has been attributed to the presence of oxygen vacancies and strain [33]. Thus, the two mentioned above defect-based mechanisms, (i) and (ii), can contribute to the 2DEG effect but mediate it differently. With increase of interfacial defects for each of the Sr substitutes and O vacancies, these two mechanisms act oppositely. The Sr/La intermixing larger than of 30%, for instance, can completely destroy the 2DEG, as we show below.

The main goal of our current study is to investigate the impact of long-range disorder on the 2DEG properties at oxide interfaces. Up to now, only a very limited number of experimental and theoretical papers were published on this topic. A strong cation La/Sr and La/Al intermixing was observed in epitaxial (3–5 u.c.) LAO/STO heterojunctions prepared with off-axis pulsed laser deposition (PLD) technique [19,20]. The degree of intermixing and its impact on the valence band formation was experimentally traced for various film thicknesses using a high-resolution x-ray photoelectron spectroscopy, which reveals the absence of the band bending in the films. First-principles simulations found a total-energy gain due to intermixing dependent on the LAO film thickness and on the type and position of the atoms involved in the site exchange [19,20]. The calculations demonstrated as well the elimination of the interface dipole for energetically most stable intermixed configurations. In another work, various intermixing effects were induced in a controllable way to study which type of the intrinsic defects can lead to the 2DEG formation at the LAO/STO interface [21]. The experiment and first-principles calculations reveal that only Al-rich $LaAlO_3$ results in a 2DEG formation, since in this case the diffusion of the cations away from the interfaces is avoided and therewith an electronic reconstruction occurs. In the same time, in La-rich films, the intrinsic defects force cation vacancies to move to the interface, which leads to a compensation of the diverging potential. Certain types of defects can be induced by the polar discontinuity itself as it was shown using first-principles simulations [22].

All the studies were performed using a supercell approach, which assumes short-range nature of defects by the construction. Moreover, the choice of the defect concentration and its positions at the interface is strictly limited by the large size of such a problem. A coherent potential approximation (CPA) offers an alternative and elegant way to describe defects or impurities using a self-consistent Green function formalism [34]. Such a method can be applied for homogeneously distributed disorder of any concentration within a conventional unit cell. Thus, the approach can adequately describe LAO/STO or similar interfaces, which are characterized by moderate cation intermixing and oxygen vacancies arising during the sample preparation. Although a CPA method can not take into account structural relaxations around a single defect, it is possible to mimic relaxations of one or more sublattices (relaxations of long-range order). Although structural relaxations could strongly affect the 2DEG formation [14], a recent surface x-ray diffraction experiment did not find any significant atomic displacement at a properly prepared interface (in particular $LaFeO_3/SrTiO_3$) [12]. In the same time, scanning transmission electron microscopy measurements, carried out on the same sample, show substantial cation intermixing at the interface. The structural relaxations can be avoided by thermal treatment, which can lead even to an additional cation intermixing, decreasing potential barriers and raising mobility of the atoms. This indicates the thickness dependence of an insulator-to-metal transition might be also explained by chemical aspects of disorder. In reality, both scenarios may happen with different importance depending on the sample quality and experimental conditions. Nevertheless, in our work we show that not only relaxations but also intermixing itself and other defects might strongly affect the 2DEG properties. Neglecting structural relaxations in our consideration enables to understand the impact of the cation intermixing and oxygen vacancies on the formation of 2DEG.

The contemporary density functional theory within a coherent potential approximation can adequately describe the electronic structure of complex interfaces with multiple defects [12,35]. Meanwhile, the insulating band gap, which is typically underestimated from first principles, can be treated up to its experimental value by utilizing a Hubbard parametrization [36], a hybrid functional, or GW approximation. Regarding the LAO/STO (001), this interface can be dually terminated, namely, either LaO/TiO_2 (LT) or AlO_2/SrO (AS). Experimentally, it is well established that perovskites grow in complete unit cells on an atomically clean and TiO_2-terminated substrate [37]. Thus, the top termination of LAO should be AlO_2 unavoidably. For that reason we calculate simultaneously the both terminations, LT and AS, using a superlattice geometry. That allows to see how the system screens off the chemical potential mismatch between the two materials. One can illustrate, therefore, how the valence and conduction band edges vary toward the interface and how the electron (hole) carriers appear in the gap, within few interfacial u.c., for the LT (AS) termination, respectively. Recently, the two-dimensional

hole gas (2DHG) formed at the AS-terminated LAO/STO was investigated both experimentally and with first-principles simulations [38]. For this termination, the metallic density of states was studied from first-principles already before by Park *et al.* [39]. Here, we calculate and compare the carrier effective masses of 2DEG and 2DHG that allows to speculate why the observation of 2DHG is obscure.

Moreover, inspecting the (110) and (111) interfaces of LAO/STO, we reveal the compulsory conditions needed to develop a 2DEG. The issue of the (110) and (111) geometries, which appears sometimes in literature [40], is important as well for understanding the LAO critical thickness >2 nm which results in 2DEG. We illustrate below how this critical thickness is related to the cation intermixing mechanism of 2DEG. Finally, it will be shown that the strength of 2DEG, which is attributed to the LT termination, may be tuned by defect variations near the interface and also manipulating defects on the opposite and spatially distant AS interface where holes are accommodated. Such tuning of 2DEG was not discussed previously.

II. DETAILS OF FIRST-PRINCIPLES CALCULATIONS

First-principles calculations published so far on LAO/STO used either heterostructures (periodically repeated superlattice) [39,41] or slab geometries with a separating vacuum layer, which models the presence of a surface [8,10,22,42–46]. The use of the latter, however, does not allow to keep ultrathin LAO as a well-insulating side because of a long-standing problem of polar discontinuity. Since LAO grows in complete unit cells on the TiO_2-terminated STO (001), the topmost layer of LAO is AlO_2, the composition of which differs critically from that of neutral Al_2O_3. This results in significant atomic displacements followed by electronic reconstruction at the free surface of LAO (001). That is why the use of superlattice in our work should give the reliable results regarding 2DEG. By varying the LAO thickness in LAO/STO between 2 u.c. (four atomic layers) and 12 u.c., as shown in Fig. 1, we study the thickness-dependent transition from the insulating state to 2DEG. In fact, the use of superlattice removes the most serious question concerning the electrostatic boundary conditions of free surfaces and their impact on the interface studied. The presence of a surface would definitely lead to substantial structural changes. In this work we would like to address mainly cation intermixing effects at sharp interfaces avoiding any modification of atomic positions. This reflects results of the recent experiment on LFO/STO interfaces, in which no significant atomic relaxations but strong cation intermixing were found [12].

Thus, the two terminations of LAO/STO, namely, LT and AS, were simulated simultaneously, within the supercells, the thickness of which was varied up to 12-u.c.-thick STO and LAO, as shown in Fig. 1. The in-plane lattice parameter was fixed to the experimental value of bulk STO ($a_0 = 3.905$ Å) to simulate the epitaxial growth of LAO/STO on the STO substrate. All calculations of perfect and imperfect LAO/STO were performed using a first-principles Green function method [47,48] based on the multiple-scattering theory within the density functional theory in a generalized gradient approximation (GGA) to the exchange-correlation potential [49]. We used a full charge-density treatment to take into account the possible nonsphericity of the crystal potential and the charge density. The maximal angular momentum used was $l_{max} = 3$ and the integrals over the Brillouin zone were performed using the $16 \times 16 \times 2$ k-point mesh.

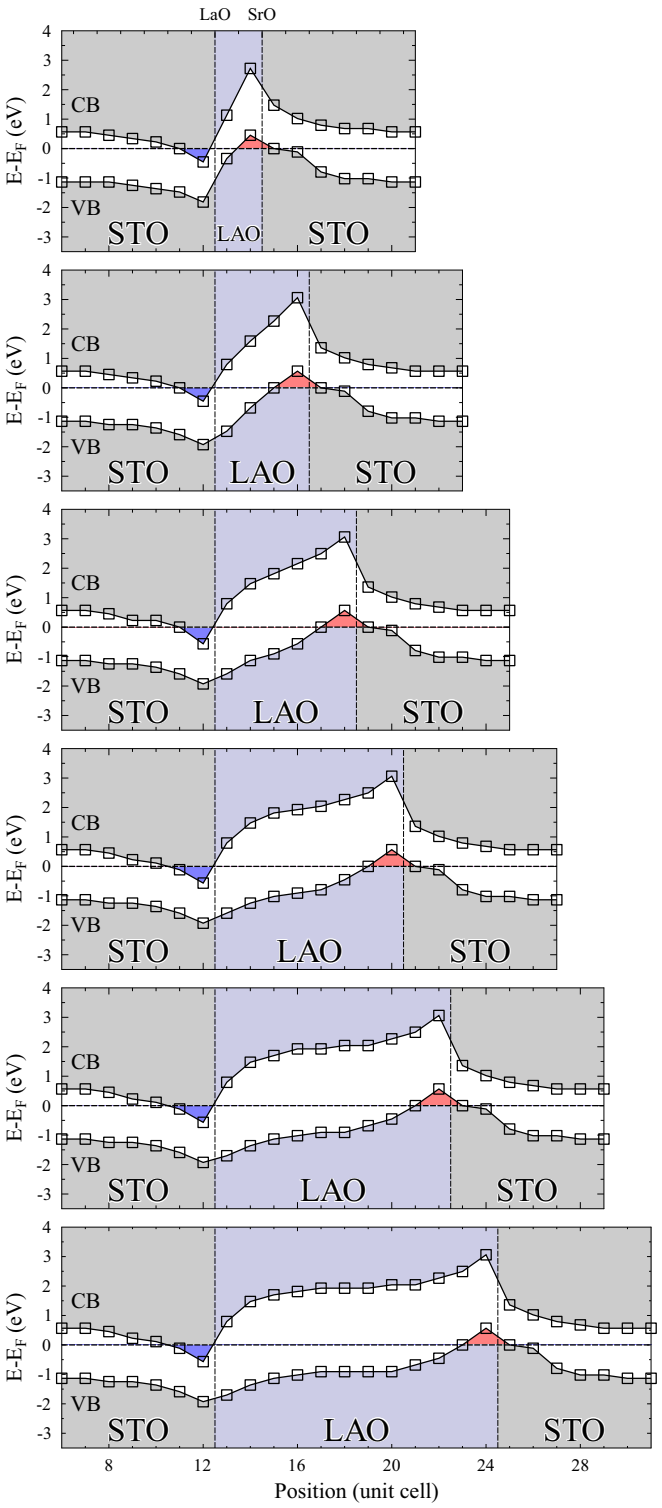

FIG. 1. The conduction/valence band profiles, calculated along the [001] direction of LAO/STO (001) superlattice and shown as a function of the LAO thickness varied between 2 and 12 u.c.

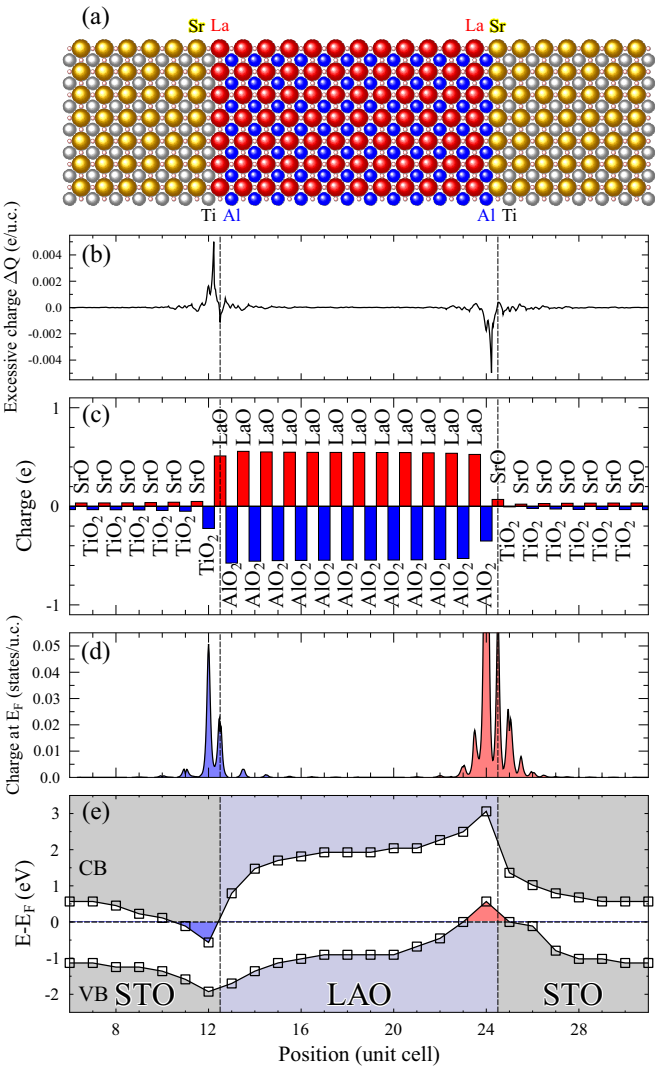

FIG. 2. Atomic structure (a), the excessive interface charges (b), discrete layer-resolved charges (c), free charges calculated at E_F (d), and the conduction/valence band profile (e) along the [001] direction of LAO/STO (001). The superlattice was constructed as the 12 u.c./12 u.c. supercell. In (a), red balls depict La atoms, blue Al, golden Sr, gray Ti, and small rose-colored balls show oxygens.

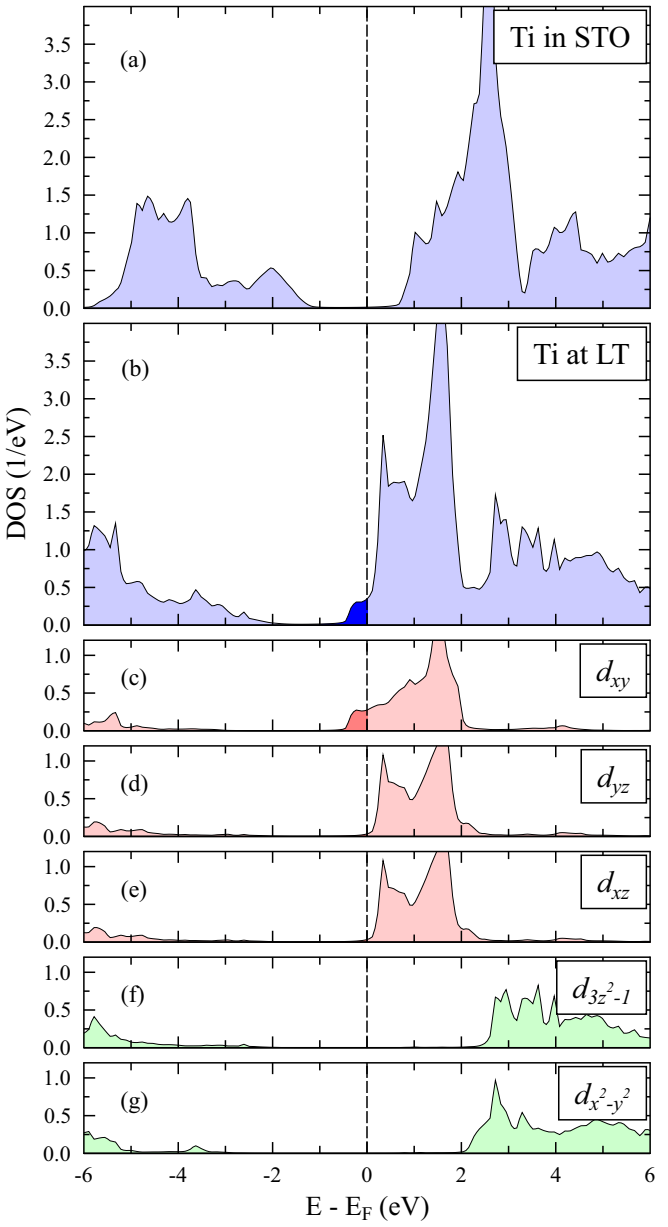

FIG. 3. Density of states (DOS) projected on selected Ti in LAO/STO (001). The total DOS of (i) the distant Ti site from the LaO/TiO_2 interface and (ii) interfacial Ti are plotted in the two top panels (a) and (b), respectively. Below, in (c)–(g), the partial ($l = 3, m$) contributions to the $3d$ states of interfacial Ti are shown.

The cation intermixing across the LAO/STO interfaces, oxygen and cation vacancies were simulated using the coherent potential approximation [34,50,51]. The oxygen vacancies were locally distributed over the oxygen sites near the interfaces. We denote these defect structures as $ABO_{3-\delta}$.

III. PERFECT LAO/STO INTERFACES

A. (001) interface

Atomically sharp and chemically perfect interfaces of LAO/STO(001) are shown in Fig. 2(a). At the interface LT, each interfacial Ti has six nearest oxygens, four next-nearest Sr, and four next-nearest La, while the interfacial Al cation placed at the AS interface has the same surroundings. Our calculations of the conduction and valence band profiles along [001] show that the 2DEG and 2DHG appear simultaneously at the LT and AS interfaces, respectively [see Fig. 2(e)]. The result was obtained using the ideal cubic perovskite structure of STO (without any structural optimization) and a conventional GGA density functional.

The polar discontinuity at both terminations of LAO should be screened. To illustrate this screening we compute the charges within Wigner-Seitz cells of each ion and then sum them over each (001) layer. Concerning the LAO side, its layers LaO and AlO_2 are both polar and charged oppositely by $\sim+\frac{1}{2}$ and $\sim-\frac{1}{2}$ electrons, respectively. The SrO and TiO_2 layers of STO are almost neutral except the interfaces. At the LT interface, the TiO_2 layer becomes negatively polarized, as is

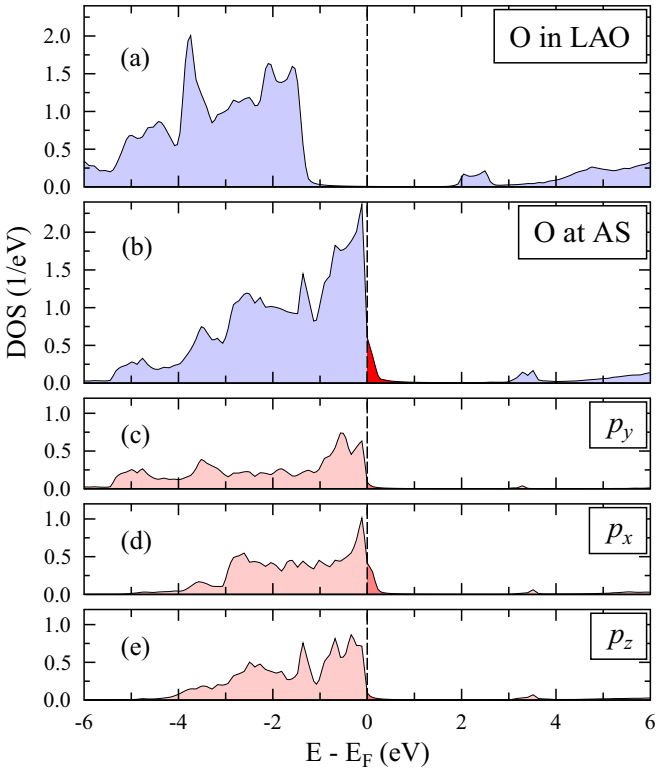

FIG. 4. The oxygen DOS in LAO/STO (001) calculated for the bulklike LAO site and interfacial O site of AlO_2 layer are plotted in the two upper panels (a) and (b), respectively. The three p-orbital DOS of interfacial O are plotted in (c)–(e).

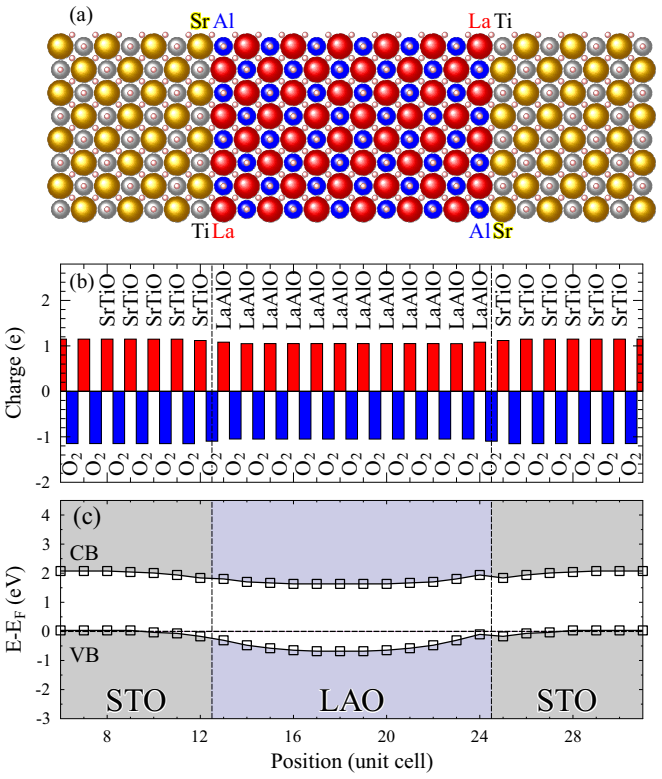

FIG. 5. Atomic structure (a), layer-resolved polarity (b), and band bending (c) in LAO/STO (110) heterostructure.

shown in Fig. 2(c) with the charge value less than a half of that of its neighboring LaO partner. This may reduce the oxidation state of interfacial Ti from typical 4+ in bulk STO to the value of 3.5+. Regarding the AS interface, one can see in Fig. 2(c) that the interfacial SrO is charged positively but insignificantly, whereas the nearest AlO_2 layer loses its negative charge by about $\frac{1}{3}$. Nevertheless, the oxidation state of interfacial Al, 3+, remains unchanged. These results agree fully with the previous first-principles and model calculations [17,52].

In Fig. 1 we plot the conduction and valence band profiles calculated along the [001] direction of LAO/STO (001) superlattices ranging between 2 and 12 u.c. The six panels of Fig. 1 show how the topmost valence band and the lowest conduction band of each u.c. of the LAO/STO (001) superlattice are changed toward the interfaces. The potential step between STO and LAO forms a band bending, which is significantly large for LAO thinner than 4 u.c. As the result, the insulating band structure of ultrathin LAO resembles that of ferroelectric perovskite polarized along [001]. The 2DEG formed between STO and a robust ferroelectric, such as $BaTiO_3$ or $PbTiO_3$, has been recently anticipated from first principles [53–55]. In accordance with our calculations, the band-bending effect at LAO/STO (001) is strong enough to develop a 2DEG for any LAO thickness. This statement, however, contradicts the corresponding measurements, which show no 2DEG effect when LAO is less than 4 u.c. One possible reason for this disagreement is a strong structural relaxation at the interface found in previous studies [10,14]. In the same time, a cation intermixing can be also responsible for depolarization effects [12,19–22]. The latter aspect will be discussed in the next section.

To elucidate the 2DEG effect at the LT interface, we calculated site-projected and layer-resolved densities of states (DOS). Figure 3 shows in the two upper panels the difference in the DOS between interfacial and another more distant Ti, which is placed in the sixth u.c. of STO starting from the interface. The DOS, $n(E)$, on distant Ti is similar to that of Ti in bulk STO. For interfacial Ti we found that its $n(E)$, which appears in the former gap below the Fermi level (E_F), is dominated by the Ti $3d_{xy}$ states, as shown in Fig. 3(c). Thus, the layer-resolved DOS at the LT interface is metallic, $n(E) > 0$, that does manifest the 2DEG.

Regarding the AS-terminated interface of LAO/STO (001) and 2DHG arisen there, we plot in Fig. 4 the total and three partial p DOS for interfacial oxygen, which is located in the topmost AlO_2 layer of LAO. In fact, the O p states form the topmost valence band of the system. Therewith, only the O p_x states of interfacial O spill above E_F and, therefore, develop the 2DHG effect. It should be noted that in each AlO_2 layer, there is another O atom, which p_y states as well contribute to the 2DHG formation. The existence of the p type was already manifested in early works [39,52]. It was also recently shown that 2DHG formation is strongly affected by various defects, e.g., oxygen vacancies [38].

There are few intrinsic factors, which can affect the 2DEG/2DHG quantitatively. In particular, since the LAO lattice parameter of 3.79 Å is less than that of the STO (001) substrate, the ∼2% tetragonal compression can affect the LAO side of LAO/STO (001). So far, we presented the results

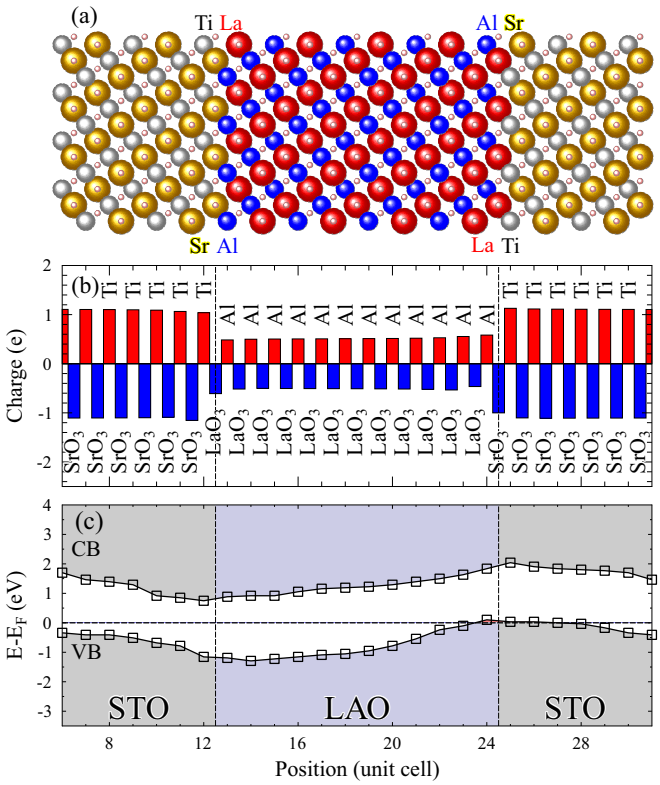

FIG. 6. Atomic structure (a), layer-resolved polarity (b), and band bending (c) in LAO/STO (111) heterostructure.

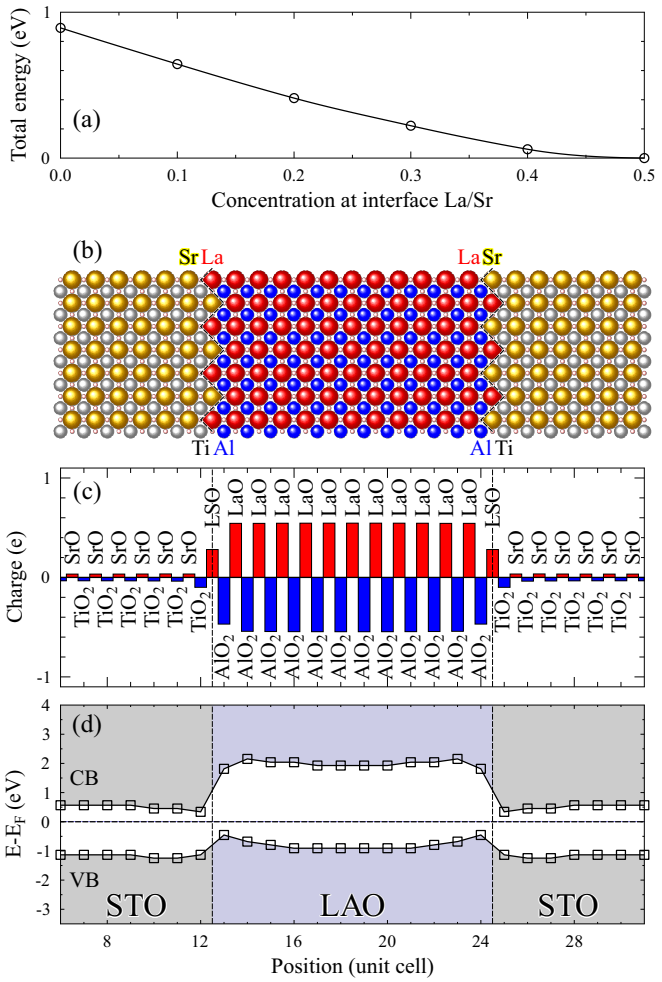

FIG. 7. Total energy of the LAO/STO (001) superlattice, which is plotted in the top panel (a) as a function of substitutional disorder x in the interfacial $La_{1-x}Sr_xO$ and $Sr_{1-x}La_xO$ layers. The panels (b), (c), and (d) show, respectively, the structure, polar discontinuity, and band profile calculated at $x = 0.5$.

obtained for the cubic perovskite structure, for which the calculated 2DEG (2DHG) carrier density, g_e (g_h), calculated at the Fermi level is 0.8×10^{13} cm^{-2} (3.4×10^{13} cm^{-2}), whereas tetragonally compressed LAO may increase the 2DEG (2DHG) effect up to 1.4×10^{13} cm^{-2} (4.3×10^{13} cm^{-2}).

Another important factor related to the 2DEG quantity evaluated from first principles is the underestimation of the band-gap size because the DFT failure. To enhance the band gap, we applied the LDA+U method on the Ti d states of STO. Increasing this parameter from $U = 0$ to 3 eV, the STO gap increases from 1.7 eV to the value of 2.3 eV. The use of $U = 6$ eV provides the band gap of 2.8 eV. Meanwhile, with increasing U the 2DEG density at the Fermi level enhances also but not linearly. For instance, for the n-type LT interface, the use of $U = 3$ eV increases g_e insignificantly from 0.8×10^{13} cm^{-2} to 0.9×10^{13} cm^{-2} whereas the U of 6 eV results in $g_e = 2.6 \times 10^{13}$ cm^{-2}, which is enhanced by 325% as compared to that of $U = 0$.

B. (110) and (111) interfaces

As next, we have modeled the band bending in ideal LAO/STO (110) and LAO/STO (111) superlattices. The corresponding results together with their polar discontinuities at the interfaces are plotted in Figs. 5 and 6, respectively. In the case of LAO/STO(110), each interfacial Ti has six next-nearest Sr and two La atoms only. The layer-resolved charges calculated along [110], which are plotted in Fig. 5(b), change smoothly at the interfaces with no polar discontinuity and, therefore, 2DEG/2DHG is not formed there since the conduction/valence bands were bent marginally. At buckled interface of LAO/STO(110), however, the 2DEG was observed and its conductivity was found to be strongly anisotropic [56]. *Ab initio* calculation which was performed to explain these foundings suggests [56] that the TiO-terminated buckled (110) surface of STO is energetically more favorable than a polar stoichiometric one. If this factor of energetics takes place, then the 2DEG can be developed at the buckled (110) LT interface because of occasional (001) islands and their stronger polar discontinuity.

Our calculations of LAO/STO (111) are illustrated in Fig. 6.

The system obeys the threefold symmetry. Interestingly, the STO (111) layers are more polar than the layers of LAO. Polar discontinuity at the interfaces, nevertheless, is not so substantial as compared to the case of LAO/STO (001). Formally, the (111) planes of STO and LAO should be strongly polar. This is shown in Fig. 6(b). However, the distances between these (111) planes of about 1.13 Å are relatively short, as compared to those of the (001) planes. In fact, the (111) layer separation is smaller than the bond length within each layer. When we

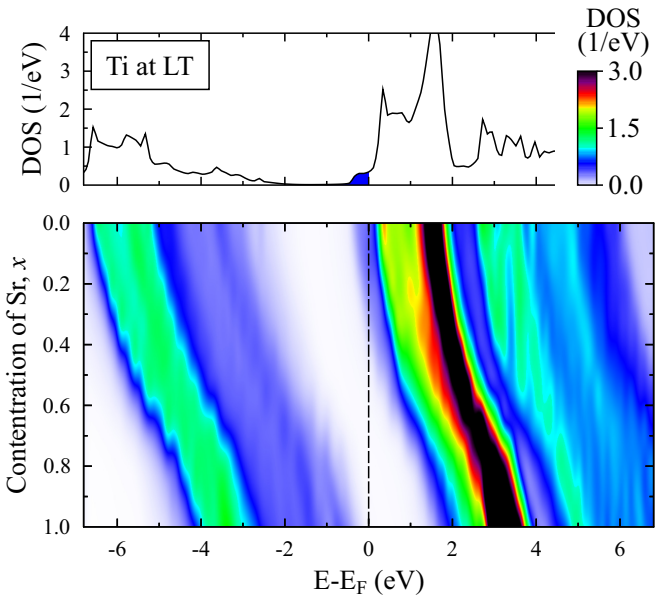

FIG. 8. DOS of interfacial Ti at the $La_{1-x}Sr_xO/TiO_2$-terminated interface of LAO/STO (001), which is mapped for $x = 0$ (top panel) and vs the Sr content x.

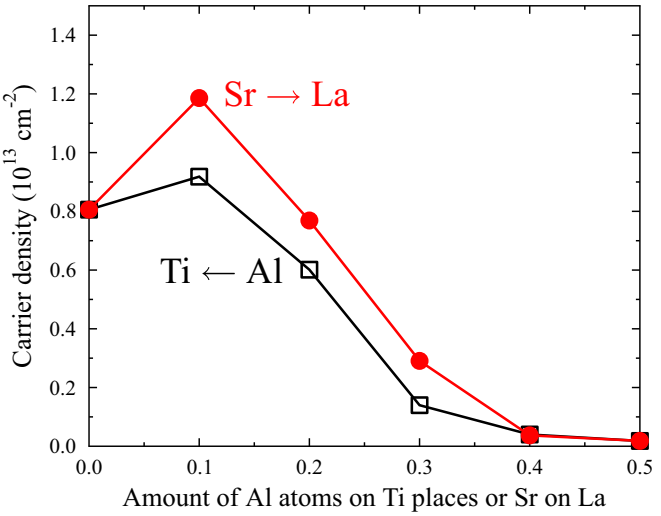

FIG. 9. 2DEG density at the Fermi level of the n-type LAO/STO (001) interface and shown by red (black) line against the Sr (Al) content x in interfacial layer $La_{1-x}Sr_xO$ ($Ti_{1-x}Al_xO_2$), respectively.

consider the charges of anions and cations projected onto the [111] direction then, obviously, the charges of nominally polar planes may compensate each other which removes polarity in LAO/STO (111). The calculated band bending, which is shown in Fig. 6(c), is more pronounced than that of LAO/STO (110) but it is significantly weaker as compared to LAO/STO (001). In a perfect LAO/STO (111), thus, the topmost valence band touches E_F but the magnitude of 2DHG is marginal while 2DEG is not presented at all.

Meanwhile, experiments report often that the (110) and (111) interfaces of LAO/STO can be made conductive with the carrier density and electronic mobility similar to those of the (001) interface [11,40]. Such a development was observed starting from critical thickness t_c of 7 and 9 MLs for (110) and (111) interfaces, respectively. The layer numbers are slightly larger there simply because the interlayer distances are reduced compared to the case of (001). In fact, all critical thicknesses needed for 2DEG are compatible to each other: $t_c(001) \approx 16$ Å, $t_c(110) \approx 19$ Å, and $t_c(111) \approx 20$ Å.

IV. IMPERFECT INTERFACES OF LAO/STO (001)

A. Cation intermixing

1. Coherent intermixing at the two interfaces

In this section, focusing on the LAO/STO (001) interfaces, we study the defect-based mechanisms of 2DEG/2DHG. Typical imperfections, which appear frequently at the (001) interfaces of epitaxially grown ABO_3 perovskites, are the material steps where the A and B cations of one perovskite substitute the corresponding cations of another material. The step heights range usually between 1 u.c. and 2 u.c., depending on the growth conditions. Since a reliable control of sharp interface is not possible, one should keep in mind that cation intermixing across the LAO/STO interface changes the charge distribution and affects the 2DEG/2DHG formation. At the LT interface of LAO/STO (001), the first candidates for mixing are La and Sr, i.e., the A cations of the two materials. The Sr species appears largely at the La sublattice, for instance, in $La(Sr)MnO_3$. Here, we considered a coherent La/Sr intermixing, modeled simultaneously across the LT and AS interfaces by varying the Sr (La) concentration in the interfacial LaO (SrO) layer between zero and 50 at. %. The amount of each A cation is conserved in each material and, hence, one can compare the total energies of the superlattice, which were calculated as a function of the Sr content x in the interfacial $La_{1-x}Sr_xO$ layer. The result, which is plotted in Fig. 7(a), shows that the total energy decreases with increasing $x \to 0.5$ and, therefore, the

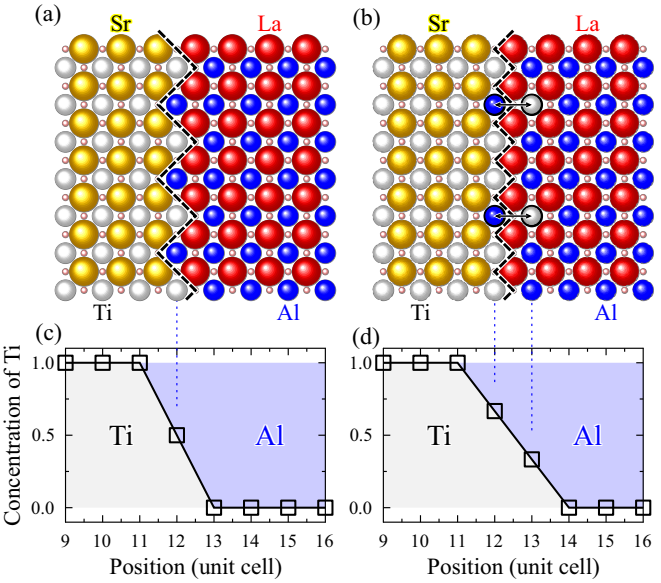

FIG. 10. Atomic structure (a), (b) and Ti/Al concentrations (c), (d) at the n-type interface for different models: (a), (c) coherent intermixing, (b), (d) single-interface cation diffusion.

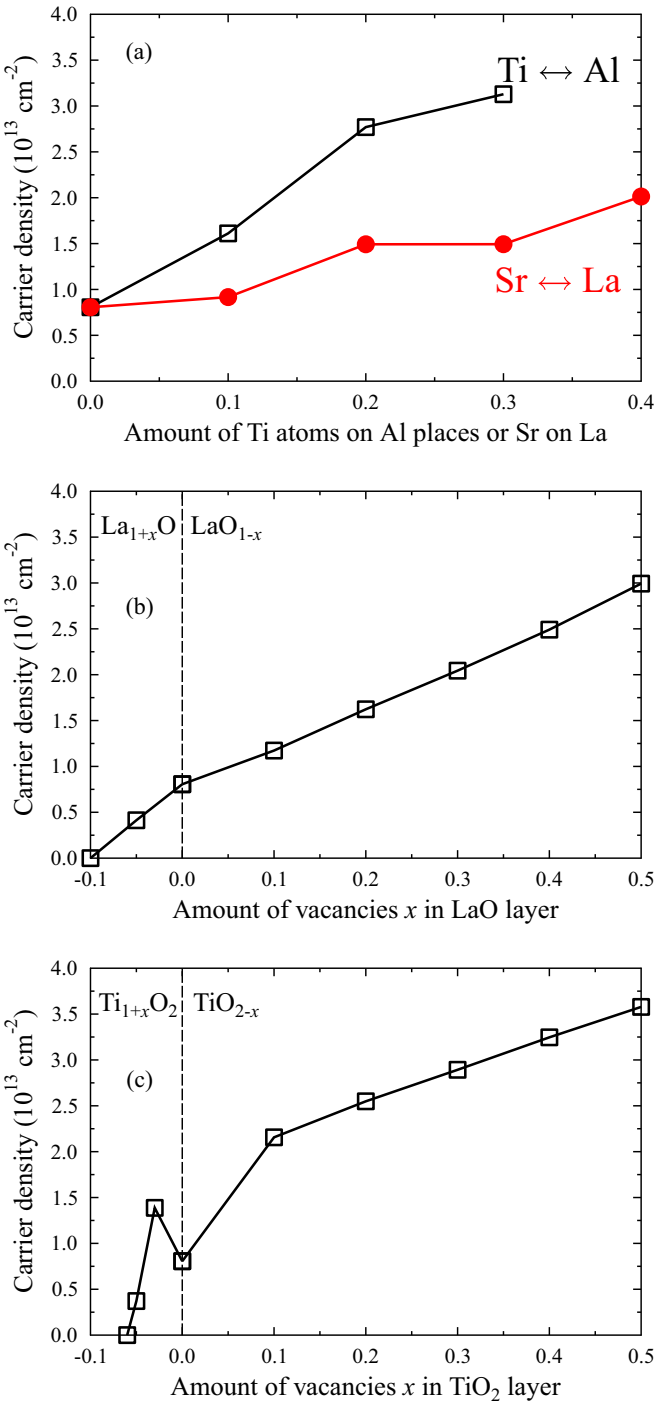

FIG. 11. 2DEG density at the Fermi energy $g_e(E_F)$, which is formed at the LT interface of LAO/STO. In (a), g_e is shown by red (black) line as a function of the A (B) cation substitutes x. In (b) and (c), g_e is plotted against the oxygen ($x > 0$) or cation ($x < 0$) vacancies in the LaO and TiO_2 layers, respectively.

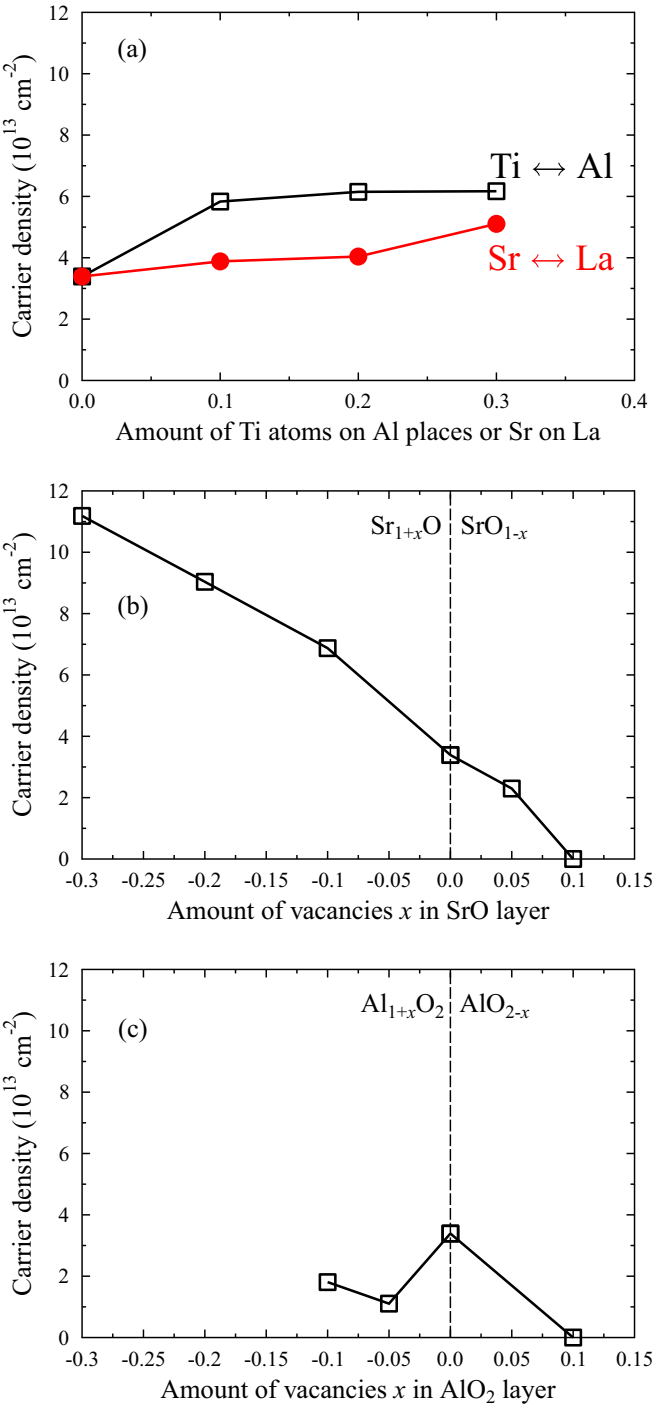

FIG. 12. 2DHG density at the Fermi level of the AlO_2/SrO-terminated interface of LAO/STO (001). In (a), g_h is shown by red (black) line as a function of the A (B) cation substitutes x. In (b) and (c), g_h is plotted against the oxygen ($x > 0$) or cation ($x < 0$) vacancies in the SrO and AlO_2 layers, respectively.

1:1 La/Sr intermixing is energetically favorable by 0.9 eV per one u.c surface area of LAO/STO (001). Most importantly, the 2DEG disappears completely at $x \to 0.5$, as shown in Fig. 7(d). This is related to the experimentally observed critical thickness of LAO of ∼1.6 nm. Although we calculated the 2DEG effect for thinner LAO up to 0.8 nm, as shown in Fig. 1, one should realize that the excessive and opposite charges of 2DEG/2DHG represent a plain capacitor, which can be broken for the LAO thicknesses below critical. Our result agrees with previous studies, in which the intermixing for $x = 0.5$ and atomic relaxations were taken into account [19,20]. However, we do not account for atomic relaxations in our study, and,

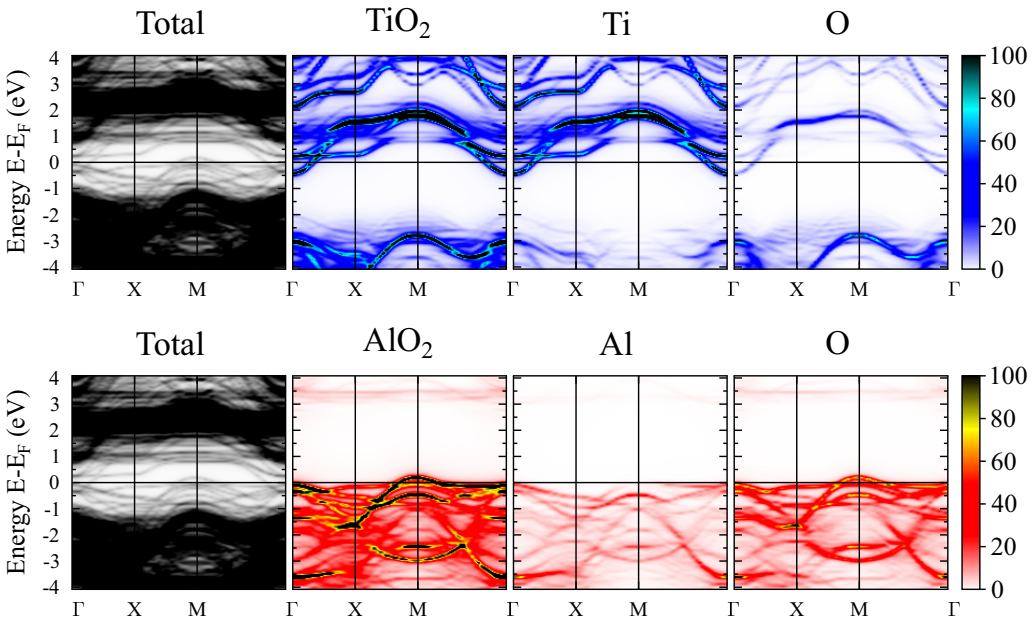

FIG. 13. Bloch spectral function, projected on the interfacial TiO_2 (AlO_2) layer of the n (p) interface of LAO/STO (001) and plotted in the upper (lower) panels along the high-symmetry directions of the 2D Brillouin zone.

therefore, can conclude that mainly the chemical intermixing leads to the depolarization of the interfaces.

To analyze the effect of coherently mixed cations at the n-type (LT) interface, we plot in Fig. 8 the DOS of the interfacial Ti vs x, namely, the Sr content in the interfacial $La_{1-x}Sr_xO$ layer. The Ti DOS of the perfect interface ($x = 0$) is shown in the top panel of Fig. 8 while its lower panel shows the change of the DOS features varying the La/Sr between $0 < x < 1$. Within the CPA approach, the Ti DOS and, in general, total DOS at the Fermi level, $n(E_F)$, completely vanishes for $x > 0.4$. For each x using the $n(E_F)$ values, we calculated the 2DEG carrier density $g_e(x)$, which is very sensitive to the DOS details near E_F. This result is shown as a red line in Fig. 9. Increasing x enhances $g_e(x)$ insignificantly at $x = 0.1$ due to the shallow Ti DOS at -0.3 eV (see Fig. 3), and then $g_e(x)$ decreases monotonically to some marginal values for $x > 0.4$. For the n-type LT interface we also modeled the B-cation step, replacing interfacial Ti by Al in the $Ti_{1-x}Al_xO_2$ layer. This result is shown in Fig. 9. The corresponding electron density $g_e(x)$, calculated at E_F as a function of the Al content, decreases with increase of x similarly to the case of La/Sr. Thus, for the LaO/TiO_2-terminated interface of LAO/STO (001) we anticipate that its 2DEG can be completely suppressed by coherently mixed cations when $x > 0.4$. It should be noted that such scenario assumes the superlattice and, therefore, needs the coherent cation mixing at the second AlO_2/SrO interface. In practice, the 2DEG is observed in the LAO/STO system which obeys the LaO/TiO_2 interface and electronically (or even chemically) reconstructed surface AlO_2 (001).

2. Single-interface cation diffusion

Next, we consider another model of the LAO/STO cation imperfections [6,21], which differs from the coherent cation intermixing discussed above. The effect of annealing may lead to diffusion of cations outward the interface. Such intermixing may take place independently from the second interface composition. We consider the simplest scenario when the interface remains atomically sharp while swapping occurs within the 2-u.c. distance, see Fig. 10. To mimic this incoherent swapping of the A or B cations, we used our Green function CPA approach. The results of our simulations are collected in Figs. 11(a) and 12(a) for the 2DEG and 2DHG interfaces, respectively.

Regarding the developed 2DEG, shown in Fig. 11(a), g_e enhances gradually with increasing x, the cation substitutes within the 2 u.c. near the LT interface. However, the 2DEG feature is more pronounced for the B-cation intermixing: Ti $\leftrightarrow$ Al. This is not surprising since 2DEG is formed by the Ti d states, as shown in Fig. 3. Similarly, the hole carrier density g_h increases also with rising the cation substitute content at the AS interface [see Fig. 12(a)]. In the case of 2DHG, the B-cation intermixing enhances g_h stronger than the A-cation intermixing. This is because the holes arise mostly in the AlO_2 layer near the AS interface and, thus, the intermixing Ti $\leftrightarrow$ Al should be more efficient in the context of g_h.

Most importantly, there is a key difference in 2DEG at the cation-substitute containing LAO/STO (001) between the coherent and incoherent (single-interface) intermixing that can be easily found by comparison of Figs. 9 and 11(a). For the latter case, its g_e increases remarkably with increasing x, whereas the two-interface coherent intermixing leads to the opposite trend and suppresses 2DEG completely at $x > 0.4$.

B. Effect of vacancies

Oxygen vacancy is the most common defect of epitaxially grown perovskite heterostructures. Here, using the Green function CPA method, we model the presence of oxygen vacancies in each interfacial layer of LAO/STO (001). As

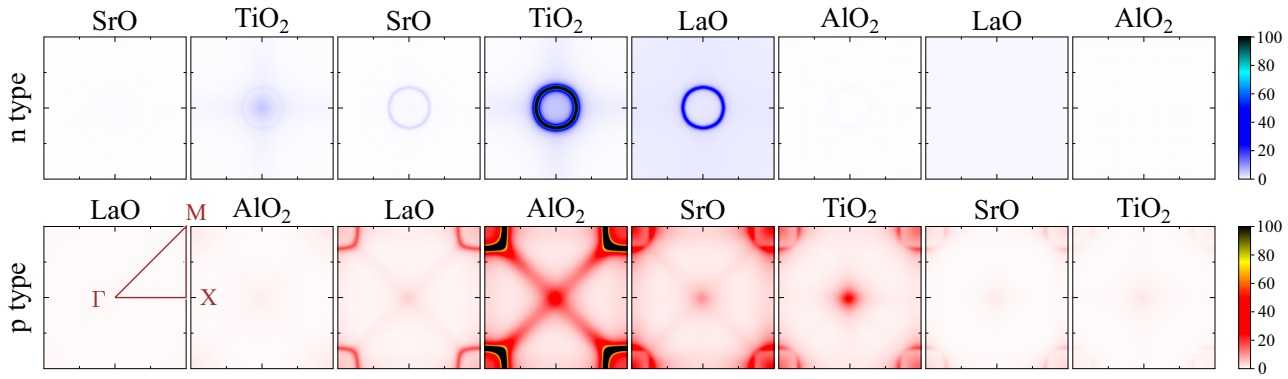

FIG. 14. The (001) cross sections of the Bloch spectral function, which was projected on the AO and BO_2 layers of LAO/STO (001) near its n (upper panels) and p (lower panels) interfaces.

expected, the O vacancy, in other words n doping, enhances the 2DEG effect at the LT interface. This is shown for $x > 0$ in Figs. 11(b) and 11(c) for the LaO_{1-x} and TiO_{2-x} interfacial layers, respectively. A cation vacancy, i.e., the p-doped LT interface, acts as p doping. The corresponding values of g_e are shown also in Figs. 11(b) and 11(c) as a function of negative x in the interfacial compositions $La_{1+x}O$ and $Ti_{1+x}O_2$. Obviously, the p doping reduces the magnitude of g_e so that 2DEG may be removed completely by the presence of Ti (La) vacancies of 5 at. % (10 at. %) at the interface.

The 2DHG effect at the AS interface may be enhanced by p doping that is shown in Figs. 12(b) and 12(c) for the case of $x < 0$. On the other hand, the O vacancies ($x > 0$) in the interfacial layers SrO_{1-x} and AlO_{2-x} suppress quickly the 2DHG effect, as shown in Figs. 12(b) and 12(c), respectively. In general, these findings agree with experimental observations, which report that the concentration of oxygen vacancies is 0.32 ± 0.06 while 2DHG was not detected [6]. In the same time, the recent experiment by Lee and coauthors demonstrates clearly that a suppression of oxygen vacancies leads to an enhancement of the 2DHG at the p-type interface [38].

V. TRANSPORT-RELATED DETAILS OF 2DEG/2DHG

To get a better insight into the electronic states, which form the 2DEG and 2DHG, we plot in Fig. 13 the Bloch spectral function, projected on the interfacial layers of LAO/STO (001) and plotted along the high-symmetry directions of the 2D Brillouin zone. At the n-type interface, as shown in the upper panels of Fig. 13, the Ti d band only crosses E_F near $k = (0, 0)$. As for the p-type AS interface of LAO/STO (001), the O p states of the valence band spill into the band gap around the M point $k = (1, 1)$.

The conduction bands, which cross E_F, are isotropic. One can see that as a spherical Fermi contour in the top panels of Fig. 14, where we plot the (001) cross sections of the Bloch spectral function projected on each atomic layer of LAO/STO near the n interface. In fact, the Ti d states from the TiO_2 layer contribute mostly to the Fermi surface cross section. The corresponding $E(k)$ is almost parabolic, as shown in Fig. 13. Thus, our estimate of the electron effective mass associated with the 2DEG is $0.38m_e$. The reported so far effective masses range between $0.41m_e$ [38,57] or $0.52m_e$ [45] and more heavier values [58].

Regarding the 2DHG bands at the p interface, the corresponding Fermi contours have fourfold symmetry. This is clearly shown in the lower panels of Fig. 14. As the result, the 2DHG effective mass is strongly anisotropic, ranging between $0.79m_e$ and $1.06m_e$, which were calculated for the M-X and Γ-M directions, respectively. Thus, we conclude that the 2DHG effective mass is two times larger than that of 2DEG. Recently, the authors of Ref. [38] calculated relatively heavy effective mass of $1.2\ m_e$.

VI. SUMMARY

We presented *ab initio* calculations of the dually terminated LAO/STO interfaces and their electronic properties, using the superlattice structural model. Interfacial cation intermixing across the interface and the presence of oxygen vacancies were modeled, within the Green function method and the CPA.

Based on our findings, we conclude that the 2DEG effect, which is arisen at the specifically terminated LaO/TiO_2 (001) interface, starts from the defect-free and atomically sharp composition while the quantity of the 2DEG can be controlled and enhanced by the presence of oxygen vacancies and substituted cations. We found as well that the depolarization of the LAO/STO interfaces can take place due to chemical effects of the intermixing. The transport-related properties of the studied system should be isotropic and governed by the electron carriers of relatively high mobility, which appear due to the d states of interfacial Ti.

Our findings can stimulate further experimental and theoretical studies, which include the Rashba effect and spin polarization of the 2DEG carriers on spin dynamics and transport properties of LAO/STO and similar interfaces with polar discontinuity.

ACKNOWLEDGMENTS

We thank M. Bibes for useful discussions. This work was supported by *Sonderforschungsbereich* SFB 762, "Functionality of Oxide Interfaces." The work of V.K.D. was supported by the National Science Center in Poland, research Project No. DEC-2012/06/M/ST3/00042.

APPENDIX: MACROSCOPIC DESCRIPTION OF THE LAO-STO INTERFACE

The electrostatics of insulators is usually formulated on the base of a macroscopic description, which includes averaging of a microscopic distribution of charges over some macroscopic volumes [59]. Correspondingly, instead of microscopic electric field **e** (we use the notations from Landau book [59]) there appear a macroscopic electric field $\mathbf{E} = \bar{\mathbf{e}}$ and an electric induction $\mathbf{D} = \varepsilon\mathbf{E}$, where ε is the dielectric constant of the substance. This macroscopic description includes boundary conditions at an interface between different insulators: $\mathbf{E}_{1t} = \mathbf{E}_{2t}$ and $D_{1n} = D_{2n}$, where indices 1, 2 label different substances and t, n refer to tangential and normal to the interface components, respectively. The above-mentioned boundary condition for the normal to interface component of induction D_n plays the key role for the macroscopic description of LAO/STO interface [60]. This condition is a direct consequence of Gauss's law and is fulfilled when the electric charge at the interface is zero.

The standard macroscopic description of a single interface between two insulators includes also a possibility of redistribution of charges near the interface, which occurs due to different work functions of different materials. Such a redistribution of charges forms a certain macroscopic profile of the charge density $\rho_{\rm ex}(z)$ in the bulk near interface and appearance of corresponding electrostatic potential $\phi(z)$, related to charge $\rho_{\rm ex}(z)$ by the Poisson equation $d^2\phi/dz^2 = -4\pi\rho_{\rm ex}/\varepsilon$.

It should be emphasized that any simple redistribution of charges near a single interface does not affect the above-mentioned boundary condition for D_n since the total electric charge near interface is still zero. Correspondingly, the resulting electrostatic potential $\phi(z)$ is a monotonic function. In its turn, this excludes the appearance of any "nib" in the profile of electron energy bands.

However, there is another possibility, which makes the LAO/STO interface really unique. Namely, instead of a simple charge redistribution near the interface, some charge can be moved from the interface to a large distance, i.e., to the opposite STO/LAO interface. It can be realized in layered STO/LAO structures. Indeed, as we will see in Fig. 2(b), which presents the result of *ab initio* calculation, there appear excess charges of different sign at two LAO/STO interfaces, corresponding to the charge transfer at a large distance. In this case, the total electric charge near each of the interfaces is nonzero, which is crucial for the boundary condition, and eventually leads to the jump of derivative of the function $\phi(z)$ [61].

It can be confirmed by considering a simplified macroscopic model. Let us assume that the macroscopic charge distribution near the interface $z = 0$ between STO and LAO layers, labeled as 1 and 2, can be approximated by

$$\rho_{\rm ex}(z) = \xi_0\delta(z) - \rho_0\left\{\theta(z)\,e^{-\alpha z} + [1-\theta(-z)]e^{\alpha z}\right\}, \quad \text{(A1)}$$

where $\theta(z)$ is the Heaviside's function. Here, the first term corresponds to the charge at the interface, whereas the second one describes the screening in the bulk. The distribution near another interface at a relatively large distance d (we assume $\alpha d \gg 1$) has a similar form but the opposite sign.

Then, using the Poisson equation we can find the potential profile and the electric field in the vicinity of $z = 0$ interface. The solution with boundary condition of $\phi_1(z) \to 0$ and $E_1(z) \to 0$ when $\alpha|z| \gg 1$ reads as

$$\phi_1(z) = \frac{4\pi\rho_0 e^{\alpha z}}{\varepsilon_1\alpha^2} \quad (z<0), \quad \text{(A2)}$$

$$E_1(z) = -\frac{4\pi\rho_0 e^{\alpha z}}{\varepsilon_1\alpha} \quad (z<0), \quad \text{(A3)}$$

$$\phi_2(z) = \frac{4\pi\rho_0 e^{-\alpha z}}{\varepsilon_2\alpha^2} + \frac{4\pi(2\rho_0 - \alpha\xi_0)z}{\varepsilon_2\alpha} + \frac{4\pi\rho_0}{\alpha^2}\left(\frac{1}{\varepsilon_1} - \frac{1}{\varepsilon_2}\right) \quad (z>0), \quad \text{(A4)}$$

$$E_2(z) = \frac{4\pi\rho_0 e^{-\alpha_2 z}}{\varepsilon_2\alpha} - \frac{4\pi(2\rho_0 - \alpha\xi_0)}{\varepsilon_2\alpha} \quad (z>0). \quad \text{(A5)}$$

The energy of electron corresponding to the variation of the band edge is $U(z) = -|e|\phi(z)$. One can present the energy in dimensionless units $\tilde{U}(z) = U(z)/U_0$, where $U_0 = 4\pi|e|\rho_0/\alpha^2$. This energy profile is presented in Fig. 15. It shows that in the macroscopic model with a nonzero electric charge at the interface the energy profile has a characteristic jump of derivative or a "nib" near $z = 0$.

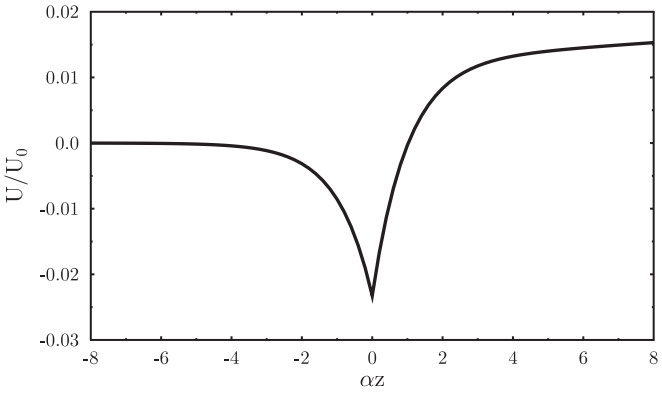

FIG. 15. Variation of the energy band edge. Here, we take $\alpha\xi_0/\rho_0 = 2.02$, and the dielectric constants of STO and LAO are $\varepsilon_1 = 43$ and $\varepsilon_2 = 28$, respectively [62].

[1] Y.-Y. Pai, A. Tylan-Tyler, P. Irvin, and J. Levy, Rep. Prog. Phys. **81**, 036503 (2018).

[2] S. Stemmer and S. J. Allen, Annu. Rev. Mater. Res. **44**, 151 (2014).

[3] M. Lorenz, M. S. R. Rao, T. Venkatesan, E. Fortunato, P. Barquinha, R. Branquinho, D. Salgueiro, R. Martins, E. Carlos, A. Liu *et al.*, J. Phys. D: Appl. Phys. **49**, 433001 (2016).

[4] A. Ohtomo and H. Y. Hwang, Nature (London) **427**, 423 (2004).

[5] S. Thiel, G. Hammerl, A. Schmehl, C. W. Schneider, and J. Mannhart, Science **313**, 1942 (2006).

[6] N. Nakagawa, H. Y. Hwang, and D. A. Muller, Nat. Mater. **5**, 204 (2006).

[7] H. Y. Hwang, Y. Iwasa, M. Kawasaki, B. Keimer, N. Nagaosa, and Y. Tokura, Nat. Mater. **11**, 103 (2012).

[8] N. Pavlenko, T. Kopp, E. Y. Tsymbal, J. Mannhart, and G. A. Sawatzky, Phys. Rev. B **86**, 064431 (2012).

[9] V. Vonk, J. Huijben, D. Kukuruznyak, A. Stierle, H. Hilgenkamp, A. Brinkman, and S. Harkema, Phys. Rev. B **85**, 045401 (2012).

[10] R. Pentcheva and W. E. Pickett, J. Phys.: Condens. Matter **22**, 043001 (2010).

[11] G. Herranz, F. Sánchez, N. Dix, M. Scigaj, and J. Fontcuberta, Sci. Rep. **2**, 758 (2012).

[12] P. Xu, W. Han, P. M. Rice, J. Jeong, M. G. Samant, K. Mohseni, H. L. Meyerheim, S. Ostanin, I. V. Maznichenko, I. Mertig *et al.*, Adv. Mater. **29**, 1604447 (2017).

[13] C. Li, Z. Liu, W. Lü, X. R. Wang, A. Annadi, Z. Huang, S. Zeng, Ariando, and T. Venkatesan, Sci. Rep. **5**, 13314 (2015).

[14] R. Pentcheva and W. E. Pickett, Phys. Rev. Lett. **102**, 107602 (2009).

[15] R. Pentcheva, M. Huijben, K. Otte, W. E. Pickett, J. E. Kleibeuker, J. Huijben, H. Boschker, D. Kockmann, W. Siemons, G. Koster *et al.*, Phys. Rev. Lett. **104**, 166804 (2010).

[16] H. Chen, A. M. Kolpak, and S. Ismail-Beigi, Phys. Rev. B **79**, 161402 (2009).

[17] H. Chen, A. Kolpak, and S. Ismail-Beigi, Phys. Rev. B **82**, 085430 (2010).

[18] H. Chen, A. M. Kolpak, and S. Ismail-Beigi, Adv. Mater. **22**, 2881 (2010).

[19] L. Qiao, T. C. Droubay, V. Shutthanandan, Z. Zhu, P. V. Sushko, and S. A. Chambers, J. Phys.: Condens. Matter **22**, 312201 (2010).

[20] L. Qiao, T. Droubay, T. Kaspar, P. Sushko, and S. Chambers, Surf. Sci. **605**, 1381 (2011).

[21] M. Warusawithana, C. Richter, J. Mundy, P. Roy, J. Ludwig, S. Paetel, T. Heeg, A. Pawlicki, L. Kourkoutis, M. Zheng *et al.*, Nat. Commun. **4**, 2351 (2013).

[22] L. Yu and A. Zunger, Nat. Commun. **5**, 5118 (2014).

[23] J. Goniakowski, F. Finocchi, and C. Noguera, Rep. Prog. Phys. **71**, 016501 (2008).

[24] C. Noguera and J. Goniakowski, Chem. Rev. **113**, 4073 (2013).

[25] N. C. Bristowe, P. Ghosez, P. B. Littlewood, and E. Artacho, J. Phys.: Condens. Matter **26**, 143201 (2014).

[26] C. Nougera and J. Goniakowski, *Oxide Materials at the Two-dimensional Limit*, Springer Series in Materials Science (Springer, Berlin, 2016), Vol. 234, p. 201.

[27] G. Singh-Bhalla, C. Bell, J. Ravichandran, W. Siemons, Y. Hikita, S. Salahuddin, A. F. Hebard, H. Y. Hwang, and R. Ramesh, Nat. Phys. **7**, 80 (2010).

[28] R. Yamamoto, C. Bell, Y. Hikita, H. Y. Hwang, H. Nakamura, T. Kimura, and Y. Wakabayashi, Phys. Rev. Lett. **107**, 036104 (2011).

[29] C. Cancellieri, D. Fontaine, S. Gariglio, N. Reyren, A. D. Caviglia, A. Fête, S. J. Leake, S. A. Pauli, P. R. Willmott, M. Stengel *et al.*, Phys. Rev. Lett. **107**, 056102 (2011).

[30] B.-C. Huang, Y.-P. Chiu, P.-C. Huang, W.-C. Wang, V. T. Tra, J.-C. Yang, Q. He, J.-Y. Lin, C.-S. Chang, and Y.-H. Chu, Phys. Rev. Lett. **109**, 246807 (2012).

[31] Z. S. Popović, S. Satpathy, and R. M. Martin, Phys. Rev. Lett. **101**, 256801 (2008).

[32] J. Park, B.-G. Cho, K. D. Kim, J. Koo, H. Jang, K.-T. Ko, J.-H. Park, K.-B. Lee, J.-Y. Kim, D. R. Lee *et al.*, Phys. Rev. Lett. **110**, 017401 (2013).

[33] A. Joshua, J. Ruhman, S. Pecker, E. Altman, and S. Ilani, Proc. Natl. Acad. Sci. USA **110**, 9633 (2013).

[34] B. L. Gyorffy, Phys. Rev. B **5**, 2382 (1972).

[35] M. Ziese, I. Vrejoiu, E. Pippel, P. Esquinazi, D. Hesse, C. Etz, J. Henk, A. Ernst, I. V. Maznichenko, W. Hergert *et al.*, Phys. Rev. Lett. **104**, 167203 (2010).

[36] J. Hubbard, Proc. R. Soc. London A **276**, 238 (1963).

[37] H. L. Meyerheim, F. Klimenta, A. Ernst, K. Mohseni, S. Ostanin, M. Fechner, S. Parihar, I. V. Maznichenko, I. Mertig, and J. Kirschner, Phys. Rev. Lett. **106**, 087203 (2011).

[38] H. Lee, N. Campbell, J. Lee, T. J. Asel, T. R. Paudel, H. Zhou, J. W. Lee, B. Noesges, J. Seo, B. Park *et al.*, Nat. Mater. **17**, 231 (2018).

[39] M. S. Park, S. H. Rhim, and A. J. Freeman, Phys. Rev. B **74**, 205416 (2006).

[40] S. Davis, V. Chandrasekhar, Z. Huang, K. Han, Ariando, and T. Venkatesan, Phys. Rev. B **95**, 035127 (2017).

[41] K. Janicka, J. P. Velev, and E. Y. Tsymbal, Phys. Rev. Lett. **102**, 106803 (2009).

[42] P. R. Willmott, S. A. Pauli, R. Herger, C. M. Schlepütz, D. Martoccia, B. D. Patterson, B. Delley, R. Clarke, D. Kumah, C. Cionca *et al.*, Phys. Rev. Lett. **99**, 155502 (2007).

[43] M. Breitschaft, V. Tinkl, N. Pavlenko, S. Paetel, C. Richter, J. R. Kirtley, Y. C. Liao, G. Hammerl, V. Eyert, T. Kopp *et al.*, Phys. Rev. B **81**, 153414 (2010).

[44] M. A. Islam, D. Saldana-Greco, Z. Gu, F. Wang, E. Breckenfeld, Q. Lei, R. Xu, C. J. Hawley, X. X. Xi, L. W. Martin *et al.*, Nano Lett. **16**, 681 (2016).

[45] H. Guo, W. A. Saidi, and J. Zhao, Phys. Chem. Chem. Phys. **18**, 28474 (2016).

[46] H. L. Zhuang, L. Zhang, H. Xu, P. Kent, P. Ganesh, and V. R. Cooper, Sci. Rep. **6**, 25452 (2016).

[47] M. Lüders, A. Ernst, M. Däne, Z. Szotek, A. Svane, D. Ködderitzsch, W. Hergert, B. L. Györffy, and W. M. Temmerman, Phys. Rev. B **71**, 205109 (2005).

[48] M. Geilhufe, S. Achilles, M. A. Köbis, M. Arnold, I. Mertig, M. Hergert, and A. Ernst, J. Phys.: Condens. Matter **27**, 435202 (2015).

[49] J. P. Perdew, K. Burke, and M. Ernzerhof, Phys. Rev. Lett. **77**, 3865 (1996).

[50] T. Oguchi, K. Terakura, and N. Hamada, J. Phys. F: Met. Phys. **13**, 145 (1983).

[51] B. L. Gyorffy, A. J. Pindor, J. Staunton, G. M. Stocks, and H. Winter, J. Phys. F: Met. Phys. **15**, 1337 (1985).

[52] R. Pentcheva and W. E. Pickett, Phys. Rev. B **74**, 035112 (2006).

[53] V. Borisov, S. Ostanin, and I. Mertig, Phys. Chem. Chem. Phys. **17**, 12812 (2015).

[54] K. D. Fredrickson and A. A. Demkov, Phys. Rev. B **91**, 115126 (2015).

[55] P. Aguado-Puente, N. C. Bristowe, B. Yin, R. Shirasawa, P. Ghosez, P. B. Littlewood, and E. Artacho, Phys. Rev. B **92**, 035438 (2015).

[56] A. Annadi, Q. Zhang, X. R. Wang, N. Tuzla, K. Gopinadhan, W. Lü, A. R. Barman, Z. Liu, A. Srivastava, S. Saha *et al.*, Nat. Commun. **4**, 1838 (2013).

[57] Z. Zhong, A. Tóth, and K. Held, Phys. Rev. B **87**, 161102 (2013).
[58] A. McCollam, S. Wenderich, M. Kruize, V. Guduru, H. Molegraaf, M. Huijben, G. Koster, D. Blank, G. Rijnders, A. Brinkman *et al.*, APL Mater. **2**, 022102 (2014).
[59] L. D. Landau and E. M. Lifshitz, *Electrodynamics of Continuous Media* (Pergamon, Oxford, 1984), Vol. 8.
[60] M. Stengel and D. Vanderbilt, Phys. Rev. B **80**, 241103 (2009).
[61] V. A. Stephanovich and V. K. Dugaev, Phys. Rev. B **93**, 045302 (2016).
[62] M. Reinle-Schmitt, C. Cancellieri, D. Li, D. Fontaine, M. Medarde, E. Pomjakushina, C. Schneider, S. Gariglio, P. Ghosez, J.-M. Triscone *et al.*, Nat. Commun. **3**, 932 (2012).